

Aerodynamic Effect on Inkjet Main Drop and Satellite Dot Placement

Shen Wang
Hewlett – Packard Co.
San Diego, CA

Abstract

With the development of inkjet technology, high-speed printing was enabled with wider printhead and/or higher carriage scan speed. Photo quality images were achieved with smaller drops and multi-level, high-resolution printing. Due to the inherent features of thermal inkjet, the aerodynamic effect will be more significant in the future inkjet development.

This paper presents the numerical simulation of the aerodynamic effect on inkjet main drop and satellite dot placement. In this model, the stationary flow and plane Couette flow were used to simplify the flow patterns underneath the printhead. Non-spherical drop shape and evaporation were neglected. Droplets were traced with the Lagrangian approach. The aerodynamic effect on main drop and satellite motion and dot placement were simulated in three simplified cases and correlated with print samples. This model can also be used to simulate the aerodynamic effect on future inkjet printing with small drops and/or with high scan speed.

Introduction

An inkjet printhead consists of a series of tiny ink firing chambers, which are aligned directly with a series of nozzles. When ink is ejected from these nozzles, the inkjet starts with a big head and a tail, as shown in Figure 1.

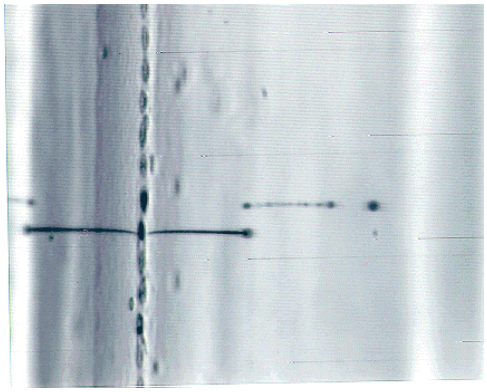

Figure 1. Drop ejection

As the inkjet travels towards the media it breaks into a main drop and several satellites. Figure 2 shows the velocity distribution of main drops and first satellites taken from a measurement of 1000 drop ejection.

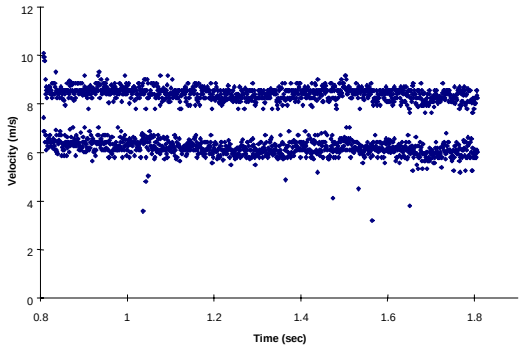

Figure 2. Velocity profile of main drops and their first satellites

The print cartridge moves in the scan axis direction during printing. If we neglect aerodynamic effects, the motion of main drops and their satellites will lie along a straight line in the direction of composite velocity of drop ejection speed and carriage scan speed. The satellites will always land away from their main drops further in the scan direction due to their longer flight time. The drops ejected from a nozzle will form similarly shaped dots on the media, irrespective of uni- or bi-directional printing.

The print samples used in this study reveal that dot shapes are different when printed bi-directionally. Figure 3 shows that drops ejected from the same cartridge have round dot shapes when the scan direction is from right to left, but have satellites next to their main drops when it scans from left to right. Analysis shows that the flow pattern underneath the printhead is different in bi-directional printing, which depends on the printer carriage configuration. The aerodynamic effect on droplet motion is associated with the flow pattern, and has a stronger influence on smaller drops. Main drop and satellite dot placement on the media will no longer be identical with bi-directional printing.

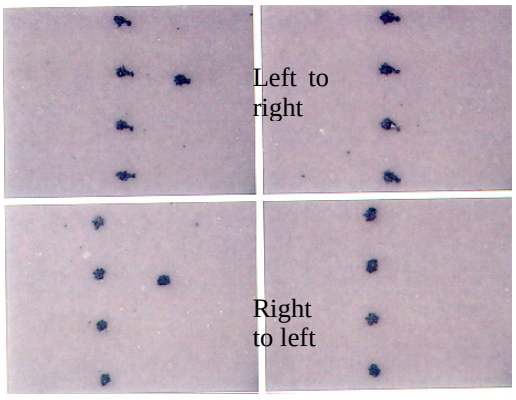

Figure 3. Dot shape in a bi-directional printing

The aerodynamic effect is also seen from print samples with forced airflow underneath the printhead. The direction of airflow is defined as from leading nozzles to trailing nozzles. Since the flow patterns underneath the leading and trailing nozzles are different, the aerodynamic effect on droplet motion will be different. Therefore, drops ejected from leading and trailing nozzles will form different dot shapes on the media, as shown in Figure 4. Using the same cartridge to repeat printing without forced airflow, drops fired from both leading and trailing nozzles formed round dots on the media. The aerodynamic effect on droplet motion is the driving force for satellites landing away from main drops in the flow direction.

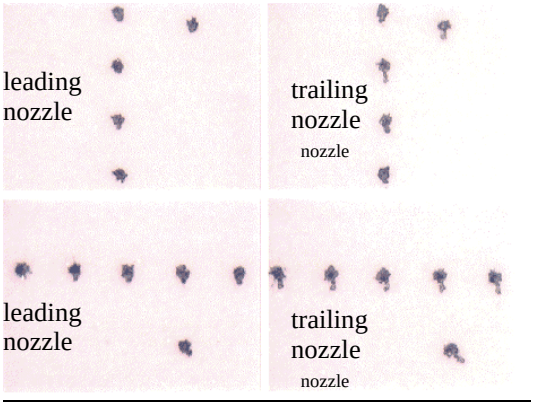

Figure 4. Dot shape printed with forced airflow

The Model

The print zone is a three-dimensional volume of space surrounding the printhead as it passes over the media during printing. Flow patterns in the print zone are very complicated. Using a two-phase flow approach, the flow patterns underneath the printhead and the governing equation for droplet motions were simplified. Droplet trajectory was traced with the Lagrangian method. There are many factors that contribute to drop trajectory error. With the focus of aerodynamic effect on droplet motion and dot placement, all the printhead defects were eliminated in this simulation. Simulation results showed that the aerodynamic force plays a dominant role in main drop and satellite motion and their dot placement on the media.

Governing Equation

The equation of motion describing the motion of an isolated droplet in a continuous fluid is the Basset-Bousinesq-Oseen equation. This equation, derived from fundamental principles by Maxey and Riley (1983), can be written for low Reynolds number as:

$$m\frac{d\vec{V}}{dt} = m_f\left(\frac{D\vec{U}}{Dt} - \vec{g}\right) + 3\pi\mu d(\vec{U} - \vec{V}) + \frac{V}{2}\rho_f\left(\frac{D\vec{U}}{Dt} - \frac{d\vec{V}}{dt}\right) + \frac{3}{2}d^2\sqrt{\pi\rho_f\mu}\int_0^t \frac{\frac{D\vec{U}}{Dt} - \frac{d\vec{V}}{dt}}{(t-\tau)^{0.5}}d\tau + m\vec{g} \quad (1)$$

where m is the mass of the isolated droplet, m_f is the mass of fluid displaced by the droplet, U is the velocity of the fluid and V is the velocity of the droplet. d/dt is the derivative associated with the isolated droplet and D/Dt is the material derivative associated with the fluid element. The first term in this analysis comes from the undisturbed flow which is due to the pressure gradient and the buoyancy force in the fluid. The next three terms come from the disturbance flow: the drag force, which is based on Stokes drag law; the virtual mass term, which represents the additional force required to accelerate the fluid; and the Basset force term which accrues from the unsteady viscous flow around the isolated droplet. The last term is gravity force.

Based on an order of magnitude evaluation, the equation of motion of a droplet can be written as

$$\frac{d\vec{V}'}{dT} = \frac{f}{St}(\vec{U}'-\vec{V}') \quad (2)$$

where the vector V' is the dimensionless instantaneous droplet velocity, vector U' is the dimensionless instantaneous velocity of local carrier fluid, and f is the modifying factor for any deviation from the Stokes drag, which is well represented for droplets with a Reynolds number less than 1000 by

$$f = 1 + 0.15\,\mathrm{Re}_p^{0.687} \quad (3)$$

where droplet Reynolds number is defined as

$$\mathrm{Re}_p = \frac{|\vec{U} - \vec{V}|\,d_p}{\nu} \quad (4)$$

ν is the fluid kinematics viscosity.

A dominant parameter for droplet motion is the Stokes number, which is defined as the ratio of droplet aerodynamic response time to the droplet flight time. The aerodynamic response time is the time required for a droplet released from rest to achieve 63% of the free stream velocity. For small values of the Stokes number, the droplet tends to follow the carrier fluid motion. For large Stokes numbers, the carrier fluid has insufficient time to influence

the droplet motion. The droplet motion will be less than that of the fluid.

Simulation Results

In this study, the main drop and its first satellite were simplified as spherical drops with Stokes numbers of 35 and 5 respectively; the time and distance of droplet motion were nondimensionalized with the flight time and nozzle to paper space. The numerical simulations were done for three simplified cases which were correlated to bi-directional printing and with forced airflow through the print zone.

Case 1: Firing drops into a stationary air environment

In the coordinate system fixed on the printer, the velocity profile of carrier flow is simplified as a step function: zero everywhere except V_c at the nozzle surface where V_c is carriage scan speed (no-slip boundary condition). The equation (2) can be written as

$$\frac{d\vec{V}'}{dT} = -\frac{f}{St}\vec{V}' \tag{5}$$

The analytic solution of this equation is

$$\vec{X} = \vec{V}_0 \frac{St}{f}(1 - e^{-\frac{fT}{St}}) \tag{6}$$

For a simulation of nozzle to paper space of *1.4mm* and a nondimensional flight time *1.4* for both main drop and satellite, the dimensional landing distance from X_0, which corresponds to the location at *T=0*, was *98um* for main drop and *69um* for satellite. Their separation, from center to center, was *29 um*. Figure 5 shows the main drop and satellite motion and trajectories. If assuming the main drop has dot size of *70um* and satellite has dot size *15um*, the satellite will overlap with the main drop.

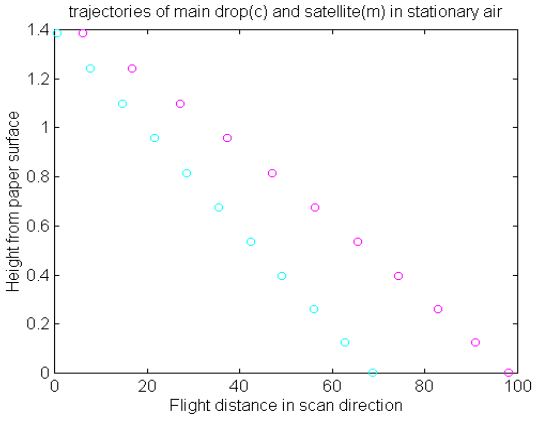

Figure 5. Main drop and satellite trajectories in a stationary air environment

Due to the aerodynamic effect, the main drop and satellite will not fly in a straight-line trajectory along the direction of composite velocity of ejection speed and scan speed. With longer flight time, the satellite tends to land away from the main drop in the scan direction. But the stronger Stokes drag force tends to push the satellite closer to the main drop. In this case, the carrier fluid velocity is zero, which means that the velocity difference between droplet and carrier fluid is greatest. Therefore, the Stokes force is the maximized, which causes the satellite dot placement to overlap with its main drop. For a certain type of printer, this case simulated the dot placement of right to left printing, as shown in Figure 3.

Case 2: Firing drop into a Couette flow

Couette flow is a simple shear flow that can be defined as the flow through the gap between paper and nozzle plate. By assuming no pressure gradient in the carrier moving direction, the equation is

$$\mu \frac{d^2U}{dz^2} = 0 \tag{7}$$

The boundary conditions for Couette flow are the no-slip condition applied to both paper and nozzle surface. The solution for this flow is a linear profile

$$U_z = \frac{V_c z}{H} \tag{8}$$

where H is the nozzle-to-paper space, z is the vertical distance from the paper, and V_c is the carriage scan speed.

There is no analytical solution for this case. The drop motion and dot placement can be numerically calculated from the following equations.

$$\vec{V}' = \vec{U}' + (\vec{V}_0' - \vec{U}')e^{\frac{-f\Delta T}{St}} \tag{9}$$

and

$$\vec{X} = \vec{X}_0 + \vec{U}'\Delta T + (\vec{V}_0' - \vec{U}')\frac{St}{f}(1 - e^{\frac{-f\Delta T}{St}}) \tag{10}$$

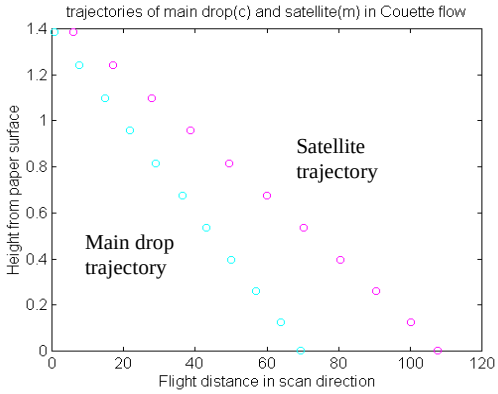

Figure 6. Main drop and satellite trajectories in a Couette flow

Using the same parameters as in Case 1, the dimensional landing distances from X_0 are *70um* for main drop and *108um* for satellite. The Stokes force has a

stronger effect on satellite motion giving a dot separation of *38 um*. The satellite will land further away from its main drop in the scan direction, as shown in Figure 6 and compared with the trajectories in Figure 5.

This case simulated the dot placement of left to right printing that was shown in Figure 3.

Case 3: With forced flow along paper axis direction

The dots in Figure 4 were printed with a low scan speed. In this simulation, a stationary cartridge was used, i.e. the scan speed was zero. The flow pattern underneath the nozzle plate was simplified as a uniform flow at the entrance (under leading nozzles) and fully developed flow at the exit (under trailing nozzles), as shown Figure 7:

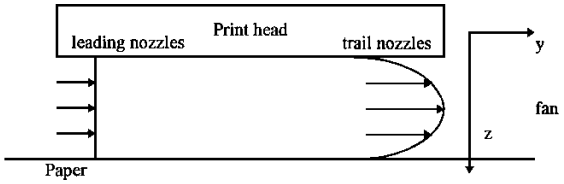

Figure 7. Flow pattern underneath leading and trailing nozzles

The velocity distribution for fully developed laminar flow is in parabolic form

$$U' = az^2 + bz + c$$
$$b.c.: z = 0, U' = 0; z = 1, U' = 1 \qquad (11)$$
$$U' = az(z-1)$$

where the nondimensional nozzle to paper space, velocity and non-slip boundary condition were used.

From the continuity equation (conservation of mass), the net flow rate of mass from the control volume is zero.

$$\rho \int_0^1 U' dz = \rho a \int_0^1 z(z-1) dz \qquad (12)$$

The equation of fully developed laminar flow can be written as

$$U'(z) = 6z(1-z) \qquad (13)$$

At *z=1/2*, flow has the maximum velocity of *1.5* unit.

The drop size parameters in this simulation are same as those used in Case 1 and 2. The velocities were nondimensionalized with the entrance velocity of forced airflow through the print zone. Dot placements were measured from the nozzle center to the dot center along the paper axis direction. The numerical simulations were run for both leading and trailing nozzle cases. The results are showed in Table 1.

Table 1. Dot placement and separation

Dot placement	Main drop	Satellite	Separation
Leading nozzle	2.7	20.0	17.3
Trailing nozzle	2.9	30.6	27.7

In a printing test, horizontal lines were printed with or without forced airflow. The line widths were then measured. Line widths were consistent from nozzle to nozzle when there was no forced airflow. Under the force airflow, the line width gradually increased from leading nozzle to trailing nozzle. As shown in Figure 8, the x-axis is from leading nozzle to trailing nozzle, top chart is the case without forced airflow and bottom chart is with forced airflow.

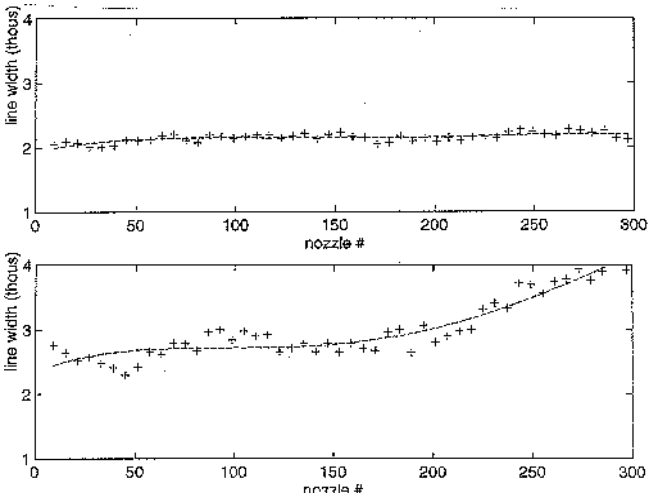

Figure 8. Line width measurement

The numerical simulation correlated well with the line width measurement. This phenomenon can only be explained with the aerodynamic effect on the dot placements of main drops and their satellites.

Conclusion

Numerical simulation is a powerful tool in inkjet product research and development. In this study, the aerodynamic effects on inkjet main drop and satellite motion and dot placement were simulated. The results correlate well with the print samples. This model can be easily adopted to simulate the small inkjet drop and fast carriage scan speed in future inkjet development. It can be used to evaluate the feasibility of a new design.

References

1. Maxey, M. R. and Riley, J.J, *Physics Fluids*, vol. **26**, pg 883-889. (1983).

Biography

Shen Wang received his Ph.D. in Mechanical Engineering from Washington State University in 1993. Dr. Wang jointed Hewlett-Packard Company Inkjet Business Unit R&D Lab in 1994. His interests include thermal and fluid dynamic effects on inkjet printing and inkjet printhead design.